RSC Advances

ROYAL SOCIETY OF CHEMISTRY

www.rsc.org/advances

Cite this: DOI: 10.1039/c0xx00000x

www.rsc.org/xxxxxx

PAPER

Aligned Carbon Nanotube/Copper Sheets: A New Electrocatalyst for CO_2 Reduction to Hydrocarbons

Youngmi Koo,[a] Rachit Malik,[b] Noe Alvarez,[b] Leon White,[a] Vesselin N. Shanov,[b] Mark Schulz,[b] Boyce Collins,[a] Jagannathan Sankar,[a] and Yeoheung Yun*[a]

Received (in XXX, XXX) Xth XXXXXXXXX 20XX, Accepted Xth XXXXXXXXX 20XX
DOI: 10.1039/b000000x

We controlled the morphologies of copper (Cu) nanostructure on aligned carbon nanotube (CNT) sheets influencing the efficiency of the electrocatalytic reduction of CO_2. Functionalized CNT sheets affected on pulsed electrodeposition of copper in terms of 3D growth, bonding, and electrochemical activity. CNT/Cu sheets electrocalyst shows high performance on electrochemical reduction of CO_2 to hydrocarbons at room temperature and atmospheric pressure. Reduction products were carbon monoxide (CO), methane (CH_4), and ethylene (C_2H_4) gases. Carbon monoxide yields (178 □ mol cm^2 mA^{-1} h^{-1}) and methane yields (346 □ mol cm^2 mA^{-1} h^{-1}) at oxygen-plasma-treated CNT/Cu sheets electrode were remarkably higher than other CNT/Cu and CNT sheets. Experimental results also show 3D morphology of copper growth on CNT sheets may play a critical role to hydrocarbon products from CO_2.

Introduction

Extrapolating efficient macroscopic materials from the individual carbon nanotubes (CNTs) that maintain and/or enhance the individual properties such as have high specific conductivity [1], chemically inert [2], high surface area [3], extremely high mechanical strength and high Young's modulus [4]. However, extrapolating these properties to macroscopic scale is still challenging. One of promising scale-up methods was recently established by multilayers of dry-spun CNT sheets [5]. Super-aligned CNT array via chemical vapor deposition (CVD) was pulled [6, 7] to highly aligned free-standing sheets of multi-walled CNTs [8, 9]. This process does not require any polymer binder and results in a flat flexible film with low density and aligned graphitic structure. Transparency and electrically conductivity of CNT sheets [10] has opened new applications including capacitors [11], batteries [12], and solar cells [13-15].

CNT sheets are electrocatalytically stable, sp^3-functionalizable, physically flexible/bendable, stackable with multilayers, much lighter than metal, self-supportable and scalable. Van der Waals forces on CNT sheets can attract CO_2 through physisorption [16]. Thus, deposition of copper on highly aligned CNT sheets can be an effective way to utilize the desirable traits of both CNT sheets and copper for electrochemical reduction of CO_2.

Metal and semi-conducting metals are well studied as electrocatalytic/photocatalytic materials for carbon dioxide reduction to hydrocarbons[17-21]. For example, copper, iron, tin, gold, and platinum as a cathode are effective electrocatalyst to reduce CO_2 to hydrocarbons and alcohols. In particular, copper is considering the most appropriate candidate for electrocatalytic processes due to its CO_2 reduction properties. Copper can electrocatalytically reduce CO_2 to hydrocarbons (mainly methane and ethylene) with reasonable current density (i.e. 5 - 10 mA/cm^2) and current efficiency (i.e. > 69 % at 0 °C) in aqueous electrolyte [17, 22]. Different atomic lattice configuration of the copper provided controllable selectivity of reduction product with higher activity [23]. Metal and semi-conducting metal-coated CNT particles are recently studied for CO_2 reduction [24, 25]. However, synthesizing metal-CNT composite particles need complex steps [26, 27] including dispersion in solvent, reaction, and drying, which need to bond to conducting substrate. These synthesized particles can break from the substrate electrode and float around (known as pulverization), so that electrocatalytic efficiency eventually decreases.

Here, we report for the first time a CO_2 reduction using electrodeposited copper nanoparticles on highly aligned CNT sheets. multi walled carbon nanotubes (MWCNT) arrays are grown using CVD, spun and stacked into a sheet. CNT sheets were pretreated through various functionalization methods and copper was electrochemically deposited. The efficiency of CO_2 reduction to hydrocarbons is investigated with CNT/Cu sheets.

Results and discussion

Assembling of CNT/Cu sheets. The CNT sheets were produced from multi walled carbon nanotubes (MWCNT) arrays using a setup built at the University of Cincinatti [8, 28] as shown in Fig. 1a. The sheets were drawn from 0.5 mm high CNT arrays, synthesized by a water-assisted chemical vapor deposition (CVD) process [6, 29, 30]. Ethylene (C_2H_4) gas was used as a carbon precursor in order to obtain spin-able CNT arrays. The synthesized CNT arrays are aligned perpendicularly to the substrate which consisted of several layers ($Si/SiO_2/Al_2O_3/Fe$ alloy catalyst). A free-standing sheet of MWCNTs was made by

pulling a bundle of nanotubes from one side of the aligned CNT array. The sheet was then attached to a Teflon™ belt and drawn at a rate of ca. 17 mm/s. The rotation of the belt causes accumulation of the formed CNT ribbon on the Teflon™ and formation of a multi-layered sheet with controllable dimensions and thickness. The array on the platforme of the setup was linearly translated by one half of its width per revolution of the belt thus allowing overlaping of the previously laid ribbon and securing lateral uniformity within the sheet. The fabricated 200 layer CNT sheets were densified layer by layer using acetone while located on the belt and exposed to tension caused by the drawing procedure. This helped to maintain the longitudinal nanotube orientation and the original dimensions obtained during densification (Fig. 1b). The 200 layer CNT sheets were characterized by scanning electron microscpy (SEM). The obtained images revealed good tube alignement and a cross-section thickness of about 10 μm (Fig. 1b and 1c). The CNT sheets were electrically connected to a 2 cm × 2 cm × 10 μm PCB (printed circuit board) and the measured end to end resistance was typically < 1 Ω from Fig. 1d. Thus, the CNT sheets can be directly used as a conductive layer of electrocatalyst for CO_2 reduction, which can simplify the fabricating process of the CNT/Cu sheets electrocatalyst. The detailed fabrications are discussed in the Methods Section.

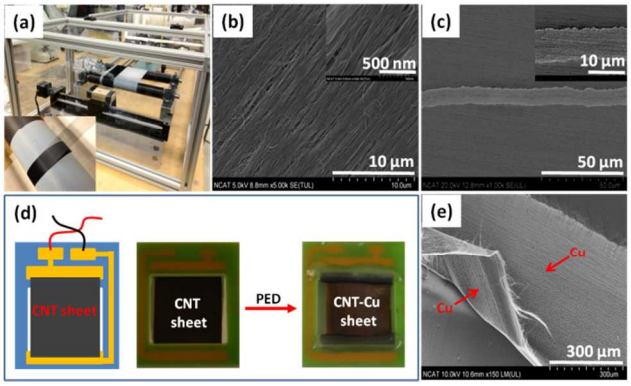

Figure 1. Fabrication of the highly aligned CNT/Cu sheets electrode. (a) Manufacturing facility for drawing of flexible CNT sheets from a vertically aligned CNT array, (b) SEM image of P-CNT sheets alignment, (c) Cross section thickness of P-CNT sheets consisted of 200 layers, (d) Schematic and pictures of O-CNT/Cu sheets electrode before and after Cu deposition, (e) Deposited Cu electrode on both sides of the O-CNT sheets.

The 200 layer CNT sheets were studied in three ways; (1) pristine CNT (P-CNT), (2) O_2 plasma treatment (O-CNT), and (3) O_2 plasma treatment and electrochemical redox cycling (OE-CNT). Raman spectra (Fig. S1) show that defect/graphite ratios (I_D/I_G ratios) of P-CNT sheets, O-CNT sheets and OE-CNT sheets were 0.83, 1.15, and 1.25 respectively [31]. The O-CNT sheets exhibit electrochemical activity of high current due to the removal of amorphous carbon and organic contaminants and reactivity of sp^3-defected sites by O_2 plasma (Fig. S2). Copper (Ⅱ) sulfate ($CuSO_4 \cdot 5H_2O$) solution (0.1 mM, pH 2.8) was used as the Cu precursor and the three different CNT sheets were pulse-electrodeposited for 5 min to obtain the CNT/Cu sheets. Fig. 1d schematically shows a CNT/Cu sheets electrocatalyst device and the Cu particles were deposited on both sides of CNT sheets well (Fig. 1e). In this work, CNT/Cu sheets were used directly without using any binder or metal current layer as an electrocatalyst.

Surface morphology of the three different CNT/Cu sheets. Fig. 2 shows morphological differences of Cu structure with three CNT/Cu sheets in terms of size, shape and distribution.

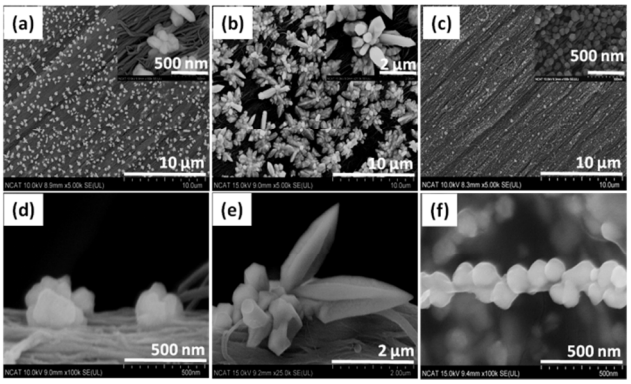

Figure 2. Scanning electron microscopy images of Cu modified on the three different CNT sheets. (a) P-CNT/Cu sheets, (b) O-CNT/Cu sheets, (c) OE-CNT/Cu sheets, (d-f) Side view of P-CNT/Cu sheets, O-CNT/Cu sheets, and OE-CNT/Cu sheets.

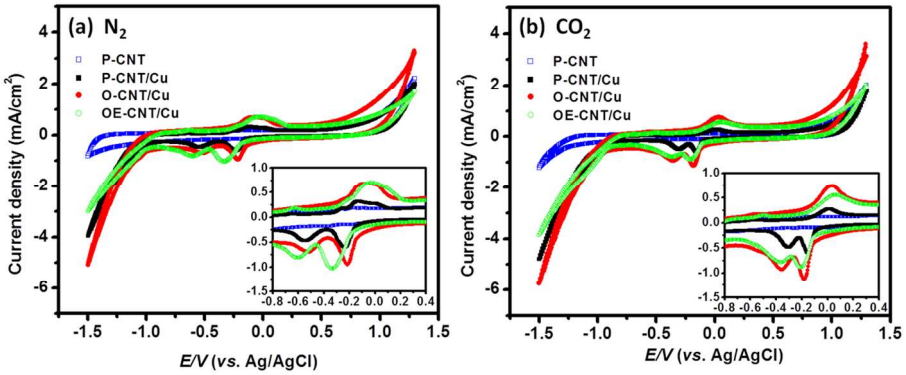

Figure 3. Cyclic voltammograms on the P-CNT sheets and the three different CNT/Cu sheets in 0.1 M $NaHCO_3$ solution at a scan rate of 10 mVs^{-1}. (a) N_2-saturated solution, (b) CO_2-saturated solution.

The Cu was deposited, coalesced and formed crystalline islands (grain formation and anisotropic growth) on P-CNT sheets and O-CNT sheets. However, the Cu of O-CNT/Cu sheets was larger and more homogeneous. Cu^{2+} ions were reduced and deposited quickly on O-CNT sheets. The presence of weakly bound oxygen atoms and oxidized defects at the CNT sheets surface created by O_2 plasma induces the formation of Cu-O bonds [32] and further promotes Cu nucleation for strong Cu pinning[33]. This was localized electrons from CNT sheets to Cu, which continue to grow Cu cluster [34]. The OE-CNT sheets were completely covered with Cu as agglomerated spheres (Fig. 2c). Electrochemically redox cycling followed by O_2 plasma might increase defect area of CNT sheets and further chemically activate the sites for Cu deposition [33, 35]. From the population density, surface area and diameter estimation from SEM images [36] (Top view of Fig. S3b (25000:1), side view of Fig. 2d-f), the Cu of P-CNT/Cu sheets shows sphere bundle shape with an average diameter of about 130 nm for spheres in each bundle. The Cu of O-CNT/Cu sheets is cylinder shape of different size, with an average diameter of about 400 nm and height 1 µm. The Cu of OE-CNT/Cu sheets shows hemisphere shapes with an average diameter of about 80 nm on the CNT sheets. Assuming these shapes and considering that Cu particles were present on both sides of the three different CNT sheets, surface areas of Cu particles were calculated to be approximately 5, 25, and 12 cm^2 respectively. The CNT sheets coverage ratios of Cu particles of each P-CNT/Cu, O-CNT/Cu, and OE-CNT/Cu are about 0.2, 0.5, and 1. We defined that coverage ratio is Cu area which is adhered to CNT sheets (covered area) to the area of CNT sheets (Fig. S3). This ratio was calculated from same SEM images. The average grain sizes are about 37.8 nm for the Cu deposited on CNT sheets calculated by using the Debye-Scherrer equation on (111), (200) reflections [37-40] from X-ray diffraction (XRD) patterns (Fig. S4). XRD pattern show that only Cu peaks were observed. The calculated deposited levels of Cu using the energy dispersive X-ray spectroscopy (EDS) are presented in Table S3. The Cu contents are 2.72 % for P-CNT/Cu, 3.0 % for O-CNT/Cu, and 30.8 % for OE-CNT/Cu sheets. The OE-CNT/Cu sheets which completely covered by Cu particles showed the largest Cu content, relatively. Though the detailed mechanism of the electrochemical formation of the Cu particles on the CNT sheets is not clear, the surface of the three different CNT sheets is believed to play an important role under the same electrochemical deposition conditions. The CNT sheets with different functionalization methods contributes to the formation of the Cu nanoparticles because the 3D network on the surface provides a large surface area as well as many electroactive sites for spatial distribution of nucleation and anisotropic growth.

Electroactivity of electrodcatalyst surfaces. Fig. 3 presents the cyclic voltammogram of P-CNT sheets and the three different CNT/Cu sheets recorded between + 1.3 and - 1.5 V without stirring in N_2 and CO_2 saturated 0.1M $NaHCO_3$ solution [19, 41-44]. The cyclic voltammograms for CNT/Cu sheets show several features including one anodic peak (O-CNT/Cu sheets in CO_2: + 0.03 V) which is indication of Cu oxide or hydroxide film formation, as well as two large cathodic peaks (O-CNT/Cu sheets in CO_2: - 0.175 V, - 0.36 V). These two peaks are attributed to the reduction of the layer formed during the anodic sweep voltammogram which results in the re-deposition of Cu [45, 46]. The voltammograms also shifted all the current-potential response in the positive direction because of the pH decrease in solution CO_2 dissolved (pH = 7.6 to 6.7)[19, 47, 48]. The results show that the current density of the O-CNT/Cu sheets was the highest. The O-CNT/Cu sheets with large activated surface area and 3D Cu clusters might provide sufficient spatial contact with large diffusion area for electrocatalytic reduction of CO_2.

Electrocatalytic reduction of CO_2. CO_2 reduction products of P-CNT sheets and three different CNT/Cu sheets were determined by various applied current in CO_2 saturated 0.1 M $NaHCO_3$ (380 mL) solution (pH 6.7). The gas products from the P-CNT sheets and three different CNT/Cu sheets are summarized in Fig. 4 and Tables S4 - S7. As shown in Fig. 4(a), small amount of hydrogen was observed for P-CNT sheets. Hydrogen evolution was not affected by total surface area of Cu particles and CNT sheets coverage ratios (Fig. S3). CO_2 by deposited Cu particles on the CNT sheets was electrocatalytically reduced to CO, CH_4, and C_2H_4 in aqueous solution. The CH_4 and CO were major products and C_2H_4 minor product in all CNT/Cu sheets. These observations are in good agreement with results of Hori et al.[49] as well as many authors [19, 50, 51], who compared the electrochemical

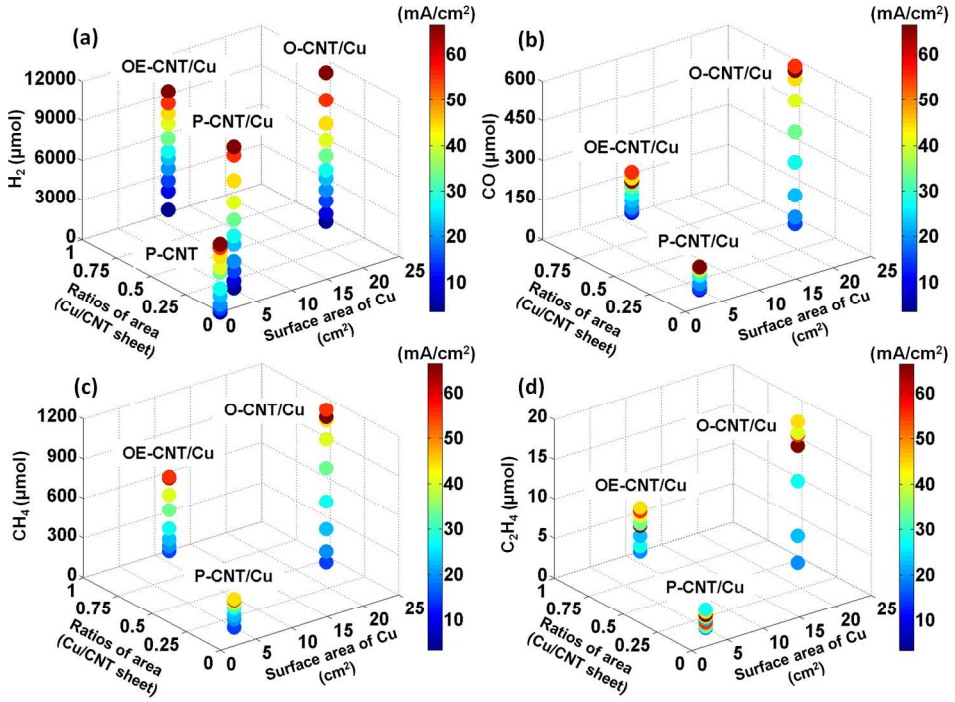

Figure 4. Electrocatalytic reaction efficiency and correlation between surface area of the deposited Cu particles and the CNT sheets coverage ratios. (a) H_2 evolution, (b) CO, (c) CH_4, and (d) C_2H_4 formation of P-CNT sheets and the three different CNT/Cu sheets in CO_2 saturated 0.1 M $NaHCO_3$ solution

reduction of CO2 to hydrocarbon at Cu electrodes. According to the literature [23], the CO_2 reduction depends on Cu's atomic configuration. On Cu (111), CH_4 formation was favored and CO formation was reduced. The C_2H_4 formation was more favorable on the Cu (100). Carbon monoxide (CO) and methane (CH_4) were found to be the major products using Cu (poly) metal foil electrode as an electrocatalysts [52-54]. As shown in the XRD results (Fig. S4), Cu particles on the three CNT sheets have a dominant Cu(111) orientation in three different CNT/Cu sheets. However, the ratio of CO_2 reduction products for these CNT/Cu sheets is very different for the structure of Cu particles on CNT sheets.

The highest reduction products were acquired from the O-CNT/Cu sheets in the range, 50 - 60 mA/cm^2. The smallest reduction products were acquired from the P-CNT/Cu electrode because of the lowest surface area of Cu particles and covered ratios of Cu particles on CNT sheets. Even though OE-CNT/Cu sheets have a large density of Cu agglomerated spheres and surface coverage (Fig. 2c), the reduction products of the CO_2 were much smaller than that of O-CNT/Cu sheets. We found that surface area of Cu particles was mainly contributed to CO_2 reduction as more impact factor than covered area of Cu particles on CNT sheets. Further, 3D structure of Cu particles might have better diffusion behavior of CO_2 to Cu/CNT sheet electrode CNT/Cu sheets could be engineered into flexible, light, stackable and scalable electrocatalytic devices for commercialization.

Conclusions

We have developed high efficient electrocatalyst using highly aligned CNT/Cu sheets. Cu morphology on CNT sheets was controlled through the functionalization for the electrocatalytic reduction of CO_2 to hydrocarbons. Reduction products were carbon monoxide (CO), methane (CH_4), and ethylene (C_2H_4) gases. CNT/Cu sheets are flexible/bendable, stackable with multilayers, reusable, much lighter than metal and scalable, which can apply for various electrocatalytic systems and devices for environmental and energy applications.

Methods

Pretreatment. To apply the O_2 plasma pretreatment and electrochemical redox cycling, the O_2 plasma treatment of CNT sheets was performed in a discharge chamber (M4L^{TM} RF gas plasma system, PVA TePla America). The 200 layered pristine CNT sheets were exposed to the plasma produced from O_2 (50 sccm) and Ar (50 sccm) gas with a nominal power of about 35 W. The pressure was fixed at 500 mTorr. Typically, the exposure lasted for 5 min. The other one has been activated by cyclic voltammetry (CV) of 10 cycles under ± 1.5 V after O_2 plasma treatment in the same condition.

Pulsed electrochemical deposition. To perform pulsed electrochemical deposition of Cu on functionalized CNT sheets electrodes, 0.1 mM $CuSO_4{\cdot}5H_2O$ was used at a pH of 2.8 and adjusted by 0.1M H_2SO_4 with KCl. Electrodeposition was performed using a potentiostat (Gamry Instrument, USA). A pristine CNT sheets with 2 × 2 × 10 μm served as the working electrode. The counter electrode was a platinum plate of 2 cm × 2 cm, and a Ag/AgCl electrode was used as a reference electrode.

The experiments were conducted at atmospheric pressure and room temperature (25 ± 1℃) and solutions were pre-purged with N_2 for 15min to remove O_2. Each CNT sheets electrode was immersed in the solution for 5 min to keep stable. The pulsed electrochemical deposition of the CNT sheets was performed at -0.8 V and 5 Hz for 5 min, which was previously determined to be the optimal duration to achieve the best eletrocatalytic performance. Finally, the CNT/Cu sheets were rinsed with DI water and ethanol.

Electrochemical reduction. The electrochemical reduction experiments were conducted in three electrode electrochemical cell. 0.1 M $NaHCO_3$ (380 mL) electrolyte was saturated with ultra pure CO_2 (99.9999 %, Airgas, USA) for 1 hour (298 K, pH 6.7). During the CO_2 reduction, the electrolyte was constantly stirred. At the end of the electrolysis after 15 min reaction, the gaseous products were immediately sampled and analyzed by gas chromatography. The gas chromatograph was equipped with a Hayesep-D and MS13X column and HID (Helium Ionization Detector) detector. Experiments for each electrocatalyst were performed after purge of one hour under a continuous flow rate of 10 mL/min CO_2 with electrochemical reduction conducted for 15 minutes. Aqueous products were not considered in this work. Data were plotted using the MATLAB.

Characterization. *Photograph*. All photographs in this work were taken with a digital camera (Nikon, D3100).

SEM. Scanning electron microscope (SEM) measurements were performed on Hitachi 8000 instrument. The images were taken in secondary electron mode with an accelerating voltage of 10 kV and working distance of 8 mm. Samples were coated with Au to prevent charging and were mounted on Al stages with conductive carbon tape.

EDS. Energy-dispersive X-ray spectroscopy (EDS) measurements were performed with Bruker AXS (XFlash detector 5030) attachment on Hitachi 8000 instrument. The images were taken in secondary electron mode, with an accelerating voltage of 10 kV, current of 10 mA and working distance of 15 mm. Samples were coated with Au to prevent charging and were mounted on Al stages with conductive carbon tape.

XRD. The X-ray diffraction (XRD) pattern was recorded using an X-ray diffractometer (Bruker, Discover D8) with Cu Kα radiation (λ = 1.5418 Å). The measurement parameters were set at 20° - 80° 2□ range, 0.014° sampling frequency, 1 sec/step scanning speed, 30 kV voltage and 40 mA current.

Raman. Raman spectra were collected by using a LabRAM ARAMIS (HORIBA Scientific). A wavelength of 633 nm (1.96 eV) He-Ne laser was used as the light source and optical filters were used to adjust the power of the laser. The area of interest on the sample surface was focused to about 2 mm.

CV. Cyclic voltammetric (CV) measurements were performed by using a potentiostat (Gamry Instruments, USA). A platinum plate was used as the counter electrode, and an Ag/AgCl electrode served as the reference electrode in N_2 and CO_2 saturated solution. Cyclic voltammetric behavior was obtained using a 10 mV/s scan rate and a - 1.5 - + 1.3 V voltage range scan limit.

Acknowledgements

This research was supported by the Office of Naval Research (N0001411103151) and the NSF Engineering Research Center (ERC) at North Carolina A&T State University. The NSF funding at the University of Cincinnati through grant SNM-1120382 is gratefully acknowledged.

Notes and references

[a] *Engineering Research Center, Department of Chemical, Biological, and Bio Engineering, North Carolina A&T State University, Greensboro, NC 27411, USA. Fax: 336 256 1153; Tel: 336 256 1151; E-mail: yyunx@ncat.edu*

[b] *Department of Chemical and Materials Engineering, University of Cincinnati, Cincinnati, OH 45221, USA. Fax: 513 556 3773; Tel: 513 556 2461; E-mail: vesselin.shanov@uc.edu*

† Electronic Supplementary Information (ESI) available: See DOI: 10.1039/b000000x/

1. T. W. Ebbesen, H. J. Lezec, H. Hiura, J. W. Bennett, H. F. Ghaemi, and T. Thio,*Nature*, 1996, **382**, 54-56.
2. A. V. V. Ellis, K. Goswami, R. N. Chakrapani, L. S. Ramanathan, P. M. Ajayan and G. Ramanath, *Nano Letters*, 2003, **3**, 279-282.
3. A. Peigney, C. Laurent, E. Flahaut, R. R. Bacsa and A. Rousset, *Carbon*, 2001, **39**, 507-514.
4. R. S. Ruoff, D. Qian and W. K. Liu, *Comptes Rendus Physique*, 2003, **4**, 993-1008.
5. M. r. D. L. Xavier Lepro´, Ray H. Baughman, *Carbon*, 2010, **48** 3621–3627.
6. M. B. Jakubinek, M. B. Johnson, M. A. White, C. Jayasinghe, G. Li, W. Cho, M. J. Schulz and V. Shanov, *Carbon*, 2012, **50**, 244-248.
7. W. Li, C. Jayasinghe, V. Shanov and M. Schulz, *Materials*, 2011, **4**, 1519-1527.
8. J. H. Pöhls, M. B. Johnson, M. A. White, R. Malik, B. Ruff, C. Jayasinghe, M. J. Schulz and V. Shanov, *Carbon*, 2012, **50**, 4175-4183.
9. H. Chen, A. Roy, J. -B Baek, L. Zhud, J. Qua, and L. Dai, *Materials Science and Engineering R*, 2010, **70**, 63-91.
10. S. F. Mei Zhang, A. A. Zakhidov, S. B. Lee, A. E. Aliev, K. R. A. Christopher, D. Williams, Ray H. Baughman, *Science*, 2005, **19**, 1215 - 1219.
11. Y. Jin, H. Chen, M. Chen, N. Liu and Q. Li, *ACS Applied Materials & Interfaces*, 2013, **5**, 3408-3416.
12. K. Fu, O. Yildiz, H. Bhanushali, Y. Wang, K. Stano, L. Xue, X. Zhang and P. D. Bradford, *Advanced Materials*, 2013, **25**, 5109-5114.
13. J. Wei, Y. Jia, Q. Shu, Z. Gu, K. Wang, D. Zhuang, G. Zhang, Z. Wang, J. Luo, A. Cao and D. Wu, *Nano Letters*, 2007, **7**, 2317-2321.
14. H. Sun, X. You, Z. Yang, J. Deng and H. Peng, *Journal of Materials Chemistry A*, 2013, **1**, 12422-12425.
15. Z. Yand, T. Chen, R. He , G. Guan , H. Li , L. Qiu and H. Peng, *Adv. Mater.*, 2011, **23**, 5436-5439.
16. F. Su, C. Lu, W. Cnen, H. Bai and J. F. Hwang, *Science of The Total Environment*, 2009, **407**, 3017-3023.
17. Y. Hori, K. Kikuchi and S. Suzuki, *Chemistry Letters*, 1985, **14**, 1695-1698.

18. M. R. Gonçalves, A. Gomes, J. Condeço, R. Fernandes, T. Pardal, C. A. C. Sequeira, and J. B. Branco, *Energy conversion and management*, 2010, **51**, 30-32.
19. J. Christophe, T. Doneux, and C. Buess-Herman, *Electrocatal*, 2012, **3**, 139-146.
20. J. Wu, F. Risalvato, and X-D. Zhoua, *ECS Trans.*, 2012, **41**, 49-60
21. C. W. Li and M. W. Kanan, *J. Am. Chem. Soc.*, 2012, **134**, 7231-7234.
22. Y. Hori, *Modern Aspects of Electrochemistry* 2008, **42**, 89-189.
23. K. J. P. Schouten, E. Pérez Gallent, and M. T. M. Koper, *ACS Catalysis*, 2013, **3**, 1292-1295.
24. J. P. O'Byrne, R. E. Owen, D. R. Minett, S. I. Pascu, P. K. Plucinski, D. Mattia, and M. D. Jones, *Catalysis Science & Technology*, 2013, 5, 1202-1207.
25. C. Genovese, C. Ampelli, S. Perathoner and G. Centi, *Journal of Catalysis*, 2013, **308**, 237-249.
26. F. Valentini, A. Amine, S. Orlanducci, M. L. Terranova, and G. Palleschi, *Analytical Chemistry*, 2003, **75**, 5413-5421.
27. S. R. Bakshi, D. Lahiri, and A. Agarwal, *International Materials Reviews*, 2010, **55**, 41-64.
28. V. Shanov, *PCT/US*, 2011.
29. L. W. Jayasinghe C, Y. Song, J. L. Abot, V. N. Shanov, S. Fialkova, S. Yarmolenko, S. Sundaramurthy, Y. Chen, W. Cho, S. Chakrabarti, G. Li, Y. Yun, M. J. Schulz, *Mas Bullentin*, 2010, **35**.
30. W. Li, C. Jayasinghe, V. N. Shanov, and M. J. Schulz, *Materials*, 2011, **4**, 1519-1527.
31. G. C. Chen, X. Q. Shan, Y. Q. Zhou, X. E. Shen, H. L. Huang and S. U. Khan, *Journal of Hazardous Materials*, 2009, **169**, 912-918.
32. C. Bittencourt, X. Ke, G. Van Tendeloo, S. Thiess, W. Drube, J. Ghijsen, and C. P. Ewels, *Chemical Physics Letters*, 2012, **535**, 80-83.
33. M. Park, B-H. Kim, S. Kim, D-S. Han, G. Kim, and K-R Lee, *Carbon*, 2011, **49**, 811-818.
34. A. Felten, J. Ghijsen, J-J. Pireaux, R. Johnson, C. M. Whelan, D. Liang, G. V. Tendeloo, and C. Bittencourt, *Journal of Physics D: Applied Physics,* 2007, **40**, 7379-7382.
35. K. T. Kim, S. I. Cha, T. Gemming, Ju¨rgen Eckert., S. H. Hong, *Small*, 2008, **4**, 1936-1940.
36. Y. Yun, V. Shanov, Y. Tu, M. J. Schulz, S. Yarmolenko, S. Neralla, J. Sankar and S. Subramaniam, *Nano Letters*, 2006, **6**, 689-693.
37. S. Wang, X. Huang, Y. He, H. Huang, Y. Wu, X. L. Lizhen Hou, T. Yang, J. Zou, and B. Huang, *Carbon*, 2012, **50**, 2119-2125.
38. V. K. Gupta, S. Agarwal, and T. A. Saleh, *Water Research*, 2011, **45**, 2207-2212.
39. S. Khabazian and S. Sanjabi, *Applied Surface Science*, 2011, **257**, 5850-5856.
40. C. Suryanarayana, and M. G. Norton, *Plenum Publishing Corporation, New York*, 1998.
41. H. De Jesús-Cardona, C. del Moral and C. R. Cabrera, *Journal of Electroanalytical Chemistry*, 2001, **513**, 45-51.
42. G. Keerthiga, B. Viswanathan, C. Alex Pulikottil, and R. Chetty, *Bonfring International Journal of Industrial Engineering and Management Science*, 2012, **2**, 41-43.
43. H. Yano, T. Akiyama, P. Bele, H. Uchida, and M. Watanabe, *Phys. Chem. Chem. Phys*, 2010, **12**, 3806–3814.
44. L.-X. W. Huan Wang, Y-C. Lan, J-Q. Zhao, and J-X. Lu, *Int. J. Electrochem. Sci.*, 2011, **6**, 4218-4227.
45. M. Jayalakshmi, and K. Balasubramanian, *Int. J. Electrochem. Sci.*, 2008, **3**, 1277-1287.
46. B. D. Smith, D. E. Irish, P. Kedzierzawski, and J. Augustynski, *J. Electrochem. Soc.*, 1997, **144**, 4288-4296.
47. Y. Hori, A. Murata, and R. Takahashi, *J. Chem. Soc., Faraday Trans.*, 1989, **1**, 2309-2326.
48. S. K. Shaw, A. Berna, J. M. Feliu, R. J. Nichols, T. Jacobc, and D. J. Schiffrin, *Physical Chemistry Chemical Physics*, 2011, **13**, 5242-5251.
49. Y. Hori, H. Wakebe, T. Tsukamoto and O. Koga, *Surface Science*, 1995, **335**, 258-263.
50. J. J. Kim, D. P. Summers, K. W. Frese Jr., *Journal of electroanalytical chemistry and interfacial electrochemistry*, 1988, **245**, 223-244.
51. J. Lee, and Y. Tak, *Electrochemica Acta*, 2001, **46**, 3015-3022.
52. K. Ogura, H. Yano, and F. Shirai,, *Fuel Chemistry Division Preprints*, 2003, **48**, 264-265.
53. W. Li, *ACS Symposium Series*, 2010, **Chapter 5**, 55-76.
54. M. Gattrell, N. Gupta and A. Co, *Journal of Electroanalytical Chemistry*, 2006, **594**, 1-19.

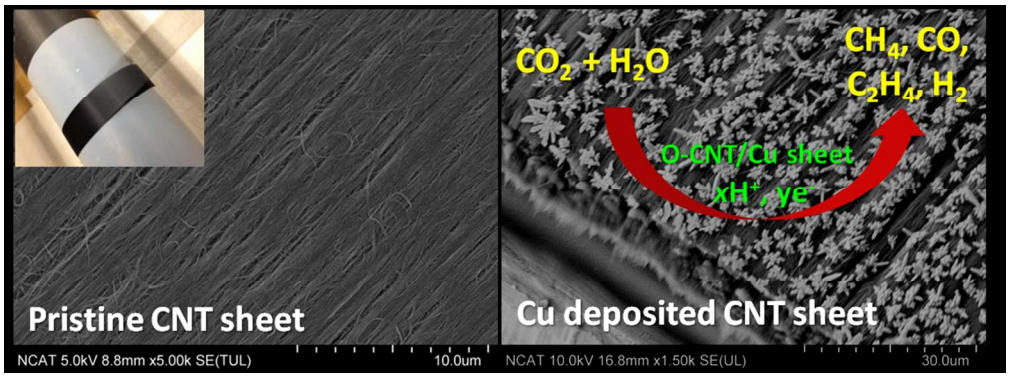

192x70mm (150 x 150 DPI)